Optimization Techniques
ME 575
March 16, 2015, Provo, USA

Journal of ME 575

DEPLOYABLE GENERALIZED CYLINDRICAL SURFACES WITH CONVEX DIRECTRICES THROUGH TAILORING STIFFNESS

Todd G. Nelson*
Compliant Mechanisms Research Group
Department of Mechanical Engineering
Brigham Young University
Provo, Utah 84604
Email: toddgn@gmail.com

Jared T. Bruton
Compliant Mechanisms Research Group
Department of Mechanical Engineering
Brigham Young University
Provo, Utah 84604
Email: jared.bruton@gmail.com

ABSTRACT

This research develops two models to form a deployable generalized cylindrical surface whose directrix, the curve perpendicular to the ruling lines of the generalized cylinder, is a convex curve. The surfaces created from using these models can be actuated from a flat state to the desired directrix curve using opposing tip loads. Such surfaces have applications in deployable reflectors and morphing wings. The first model, the continuous model, varies the bending stiffness along the directrix to create surfaces which can move from flat state to a desired generalized cylindrical surface. The second model, the discrete model, creates an approximate generalized cylindrical curved surface using a system of rigid links joined by torsional springs of varying stiffness. Compliant joints, such as the Lamina Emergent Torsion (LET) joint, can function as the torsional springs in the actual construction of these surfaces. The LET joint is suitable in this role as the joint can be planar manufactured as part of a sheet, has a relatively stable axis of rotation, and has geometry which can be adjusted to a specifiable stiffness. Such systems can have application in foldable and morphing aircraft and UAV wings, deployable antennae and reflectors, and other applications where a specific profile geometry is desired from a planar sheet.

A multidimensional optimization problem using finite element analysis is designed to verify and extend the continuous model by allowing the enforcement of constraints such as the stress in the deployed state. Another multidimensional optimization problem is defined to extend the discrete model by optimizing the geometry of the system of rigid links such that the number of joints is specified and the profile error, the area between the desired directrix and the system's approximation of the desired directrix, is minimized. Constraints can also be applied to the rigid link lengths to ensure that the joints can be physically manufactured.

The implementation of the two models and performance of the optimization routines are demonstrated through the physical construction of a deployable parabolic reflector and airfoil.

1 Introduction

The objective of this research is to present two models which can be used to create deployable generalized cylindrical surfaces. A generalized cylindrical surface is a surface that can be represented as an open generalized cylinder, one of three classes of developable surfaces. A generalized cylinder is formed by translating a straight line, called the generator line, along a path in a plane perpendicular to the generator line. The path is called the directrix of the generalized cylinder. For example, a circular directrix would give rise to the common right circular cylinder. The models in this research enable design of generalized developable surfaces where the directrix is a convex curve that does not self-intersect. Furthermore, these models are extended through optimization techniques to include constraints on various parameters to ensure the functionality and manufacturability of the surface.

Surfaces which can be controlled or predictably changed of-

*Address all correspondence to this author.

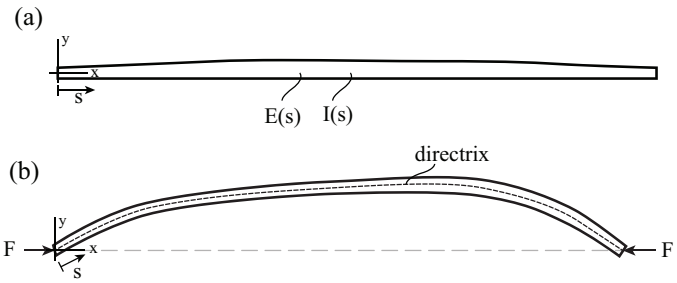


FIGURE 1. Continuous model for generating a generalized cylindrical surface showing (a) the flat position and (b) the deployed position.

fer advantages in situations where a change in occupied space or a dynamic response to an environment is desired. Origami and origami-inspired mechanisms provide examples of surfaces where a change from one state, perhaps a tightly compacted state, to another state, a deployed state, is desired. Examples of these include a deployable solar array [1], diameter-changing origami wheel [2], and origami-based heart stent [3]. Morphing wings and flight surfaces have also been investigated to create structures which can be dynamically modified to achieve geometries which perform well under varying environments or conditions [4–8]. Deployable reflectors also use the principle of morphing or changing surfaces to create the desired collection shape while still having the ability to stow compactly [9–13].

2 Method

2.1 Continuous Model for Generalized Cylindrical Deployable Surfaces

This model achieves a desired generalized cylindrical surface by continuously specifying the stiffness, or spring coefficient, along a directrix. Consider the surface shown in the flat and deployed positions in Fig. 1 where s is the arc length along the directrix, $E(s)$ is Young's modulus of the material as a function of arc length and $I(s)$ is the moment of inertia of the cross section as a function of arc length. Opposing tip loads, F, are applied to the ends of the surface to form the deployed shape. The surface's stiffness is allowed to vary continuously along the length of the directrix. Thus each generator line, a line perpendicular to the directrix, has a constant stiffness but the stiffness of one generator line can vary from the other generator lines.

To design a generalized cylindrical surface to deploy to a specified convex directrix, the curvature of the desired curve must match that curvature of the deployed surface at every point as shown in Eq. 1 and Fig. 2.

$$\kappa_{desired}(s) = \kappa(s) \tag{1}$$

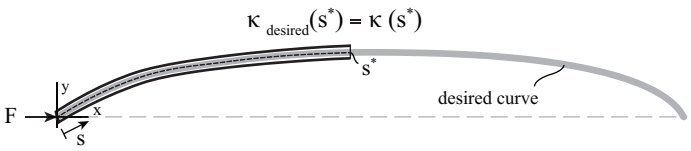


FIGURE 2. Matching the curvature of a desired curve to the generalized cylindrical surface at every point.

The Bernoulli-Euler equation states that the curvature of the surface is proportional to the bending moment applied to the surface, that is

$$M = EI\kappa \tag{2}$$

where E is Young's modulus of the material, I is the moment of inertia, and the curvature, $\kappa = d\theta/ds$, is the change in angle relative to the change in arc length along the curve..

Applying the Bernoulli-Euler equation to a the case where the stiffness is allowed to vary continuously along the directrix gives

$$M(s) = E(s)I(s)\kappa(s) \tag{3}$$

where $E(s)$ is Young's modulus of the material, $I(s)$ is the moment of inertia of the surface, and $\kappa(s)$ is the curvature of surface, each as a function of arc length.

Rearranging Eq. 3 implies that curvature can be specified by modifying the modulus of the material, the moment of inertia, the applied moment, or a combination of the three along the length of the directrix of the surface. In this research a single material with uniform material properties is used to construct the surface. Likewise, the moment at each point is determined by opposing tip loads, which could simulate a linear actuation force such as a spring, and thus will not be intentionally modified to achieve the matching curvature. Thus, for this work modification of the moment of inertia will be the vehicle for varying the stiffness and consequently curvature of the surface in the deployed state.

The moment caused by the tip loads at a point along the arc length, $M(s)$, can be found by balancing the forces as shown in the free body diagram in Fig. 3 and expressed as

$$M(s) = Fy(s) \tag{4}$$

where $y(s)$ is the height of the deployed structure as a function of arc length.

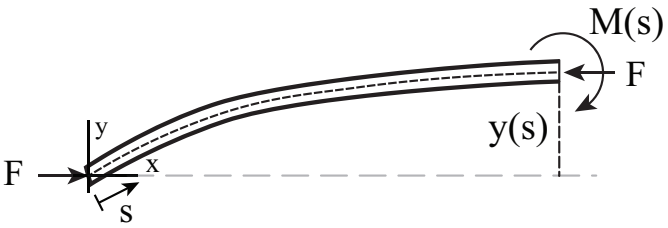


FIGURE 3. Free body diagram of the continuous model used to find the moment along the curve.

The desired curvature of the surface can be expressed in terms of the loading, material properties, and geometry of the surface using appropriate substitutions from Eq. 1, 3, and 4 as

$$\kappa_{desired}(s) = \frac{Fy(s)}{E(s)I(s)} \tag{5}$$

An example of using the continuous model to design a deployable generalized cylindrical surface with variable stiffness achieved by changing the moment of inertia will be shown here to demonstrate the method. Consider the desired deployed directrix of an inverted parabola that is described by the function

$$f(x) = -0.03(x-5)^2 + 0.75 \tag{6}$$

over the domain $x = [0, 10]$. This function is shown along with physical prototypes in Fig. 4. Opposing tip loads, F, will be used to actuate the surface and so Eq. 3 describes how the moment load varies with arc length. The material of the surface will be kept constant, resulting in a constant modulus, E. Furthermore, a rectangular cross section will be enforced with a constant base, b, and variable height, $h(s)$, as a function of the arc length of the directrix. The moment of inertia as a function of arc length is then $I = bh(s)^3/12$. Eq. 5 can be solved for $h(s)$ with appropriate substitutions as

$$h(s) = \left[\frac{12Fy(s)}{bE\kappa_{desired}(s)}\right]^{1/3} \tag{7}$$

This equation can be evaluated by using the desired directrix function, Eq. 6 to compute the desired curvature, $\kappa_{desired}(s)$, and moment arm heights, $y(s)$. The arc length formula shown in Eq. 8 can be used to relate the function in x to the arc length, s, for the desired curvature and moment arm heights.

$$s = \int_0^x \sqrt{1 + (dy/dx)^2}\, dx \tag{8}$$

Calculating $h(s)$ with $F = 2$ lb, $E = 400$ ksi, and $b = 0.115$ inches, results in the variable height rectangular beam shown in Fig. 4. The deployed state is also shown and correlates well to the desired directrix parabolic shape.

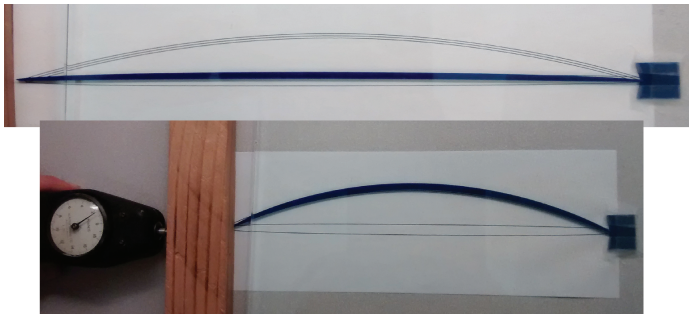


FIGURE 4. Acrylic Model Using the Analytic Solution for the parabola expressed by Eq. 6 in the flat and deployed positions.

2.2 Discrete Model for Generalized Cylindrical Deployable Surfaces

The discrete model for creating generalized cylindrical deployable surfaces uses a system of rigid links joined by torsional springs that is actuated from a flat state by opposing tip loads to form a desired directrix in a deployed state. Similar to the continuous model the geometry of the desired directrix is used to calculate the stiffness of the torsional springs between each rigid link.

Let L_1, L_2,...,L_{n-1} be the lengths of $n-1$ rigid links in the system. Let k_1,k_2,...,k_n denote the stiffness of the torsion springs between the rigid links as shown in Fig. 5(a). By placing the rigid link system in the desired curved shape where all of the endpoints of the rigid links lie upon the curve, the deployed link angles θ_1, θ_2,..., θ_n as well as the deployed heights y_1,y_2,...,y_n can be determined as shown in Fig. 5(b).

With the system of rigid links in the desired curved shape the moment at the i-th joint, M_i, can be expressed as

$$M_i = k_i\theta_i \tag{9}$$

The free body diagram drawn for the i-th joint in Fig. 6 with opposing tip loads, F, shows that the moment, M_i, can also be

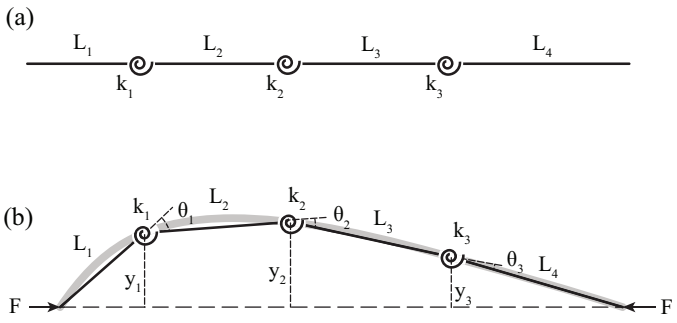


FIGURE 5. Discrete Model showing (a) a flat position and (b) an actuated position for a rigid link system of $n = 3$.

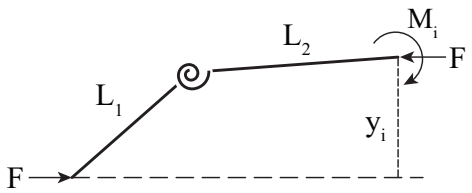


FIGURE 6. Free-body diagram of the structure cut at the i-th joint

expressed as

$$M_i = F y_i \tag{10}$$

By setting Eq. 9 and 10 equal to each other we can find an expression for the stiffness of each torsion spring in terms of known geometry

$$k_i = \frac{F y_i}{\theta_i} \tag{11}$$

Lamina Emergent Torsion (LET) joints are one candidate to implement with the discrete model. LET joints can be chained together to form a series of torsion bars serving as the torsion springs in the model. An example of the geometry of a LET joint chain used in this research is detailed in Fig. 7 where four torsion springs and five rigid links are shown. LET joints are well suited to the discrete model as the joint can be planar manufactured as part of a sheet, has a relatively stable axis of rotation at the torsion bars, and has geometry which can be easily modified to change the stiffness of the joint in a predictable way using a spring model developed by Jacobsen et al. [14]. For example, the length and width of the torsion bars can be changed to specify a certain stiffness.

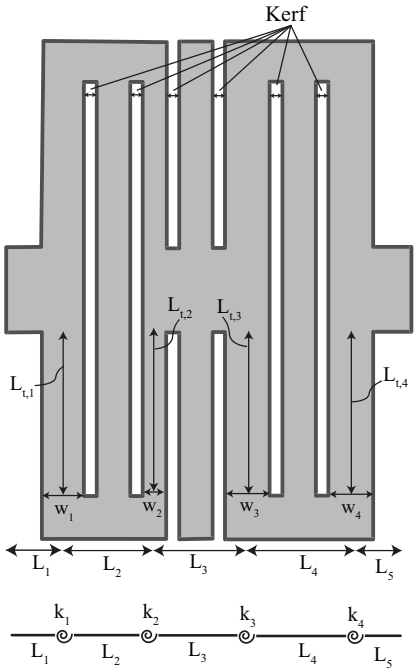


FIGURE 7. A chain of LET joints with important dimensions shown with the corresponding discrete model schematic shown below. This chain has five rigid links and four torsion springs

3 Extension of Models Through Optimization

Multidimensional optimization can be used to expand both models by allowing for the introduction of constraints to the design problem. For the continuous model a multidimensional optimization problem using finite element analysis is defined which can verify the analytical model and extend the model to accommodate constraints such as maximum stress in the deployed shape. A multidimensional optimization problem is also defined to extend the discrete model in a way that for a specified number of rigid links the profile error, or error between the desired directrix and actual directrix of the deployed surface, is minimized by efficiently locating the positions of the torsion bars.

3.1 Extending the Continuous Model

While the continuous model allows for an analytic computation of a deployable generalized cylindrical surface, constraints such as maximum allowable stress and deflection under pressure loads or other combinations of loads are difficult to incorporate into the model. Finite element analysis in conjunction with a multidimensional optimization routine allow for these constraints to be enforced in the design of the deployable continuous generalized cylindrical surface.

Consider again the example where the height of a rectangular cross section beam is allowed to vary to create a variable

stiffness surface under a tip load. The beam can be approximated in a finite element program using beam elements (ANSYS Beam 188) with linearly tapered sections between control points. Let n be the number of control points used to create the beam model with h_i being the height of the rectangular cross section at the control point for $i = 1$ to n as shown in Fig. 8. Displacement boundary conditions are placed on the nodes at each end of the beam to create the equivalent of a pinned-pinned condition. The beam is then loaded in two steps. The first step applies a moment to the beam to bias the surface towards one bending direction. This is done because directly applying opposing tip loads results in only axial compression of the beam as it is initially in a unstable, yet equilibrium condition. The second load step removes the moment load, from the now biased shape, and applies opposing tip loads to push the beam into its final deployed shape.

The optimization problem can be defined as a minimization of the profile error, the error between the desired directrix and the deployed directrix at the control points, where the design variables are the heights of the cross sections at the control points. The objective function to be minimized is defined as

$$J(h) = ProfileError = \sum_{i=1}^{n} \left(y_{desired,i} - y_{actual,i}(h)\right)^2 \qquad (12)$$

where h is the vector of cross sectional heights at n control points, $y_{desired,i}$ is the desired height of the i-th node, and $y_{actual}(h)$ is the actual height of the i-th node when the beam is actuated under tip loading as a function of the design variables. The cross sectional heights are required to stay within bounds defined as

$$lowerbound_i \leq h_i \leq upperbound_i \quad where\ (i = 1, ..., n) \qquad (13)$$

The bounds can be determined for each particular application by examining manufacturing feasibility or space requirements. For the applications in this research, engineering judgment based on prior prototype manufacturing experience was used to estimate appropriate upper and lower bounds. A yield stress constraint can be imposed to prevent plastic deformation of the deployed beam as

$$|\sigma_{max}| \leq \sigma_{yield} \qquad (14)$$

Other constraints can potentially be added to the optimization problem such as a deflection constraint under a particular loading condition, based on the needs of the problem at hand.

While this optimization problem can be solved using various gradient or gradient free methods, a gradient-free method is a useful method to obtain a reasonable preliminary solution and then a gradient method is well-suited to refine the solution. This multi-step approach is used to take advantage of the robust quality of the gradient-free method at the beginning of the optimization procedure and then the faster convergence rate and increased accuracy of a gradient method near the end of the procedure. A gradient-free method allows for a robust solver as a penalty can be added to the fitness of finite element models which fail to converge, a common occurrence at the beginning of the optimization procedure when the design space to be explored is still comparatively large. Once a reasonable solution is found the upper and lower bounds imposed on the design variables are tightened such that nearly all the finite element models in the now constricted design space will converge when solved. At this point a gradient-based method is used to refine the solution at a much faster convergence rate than the gradient-free method.

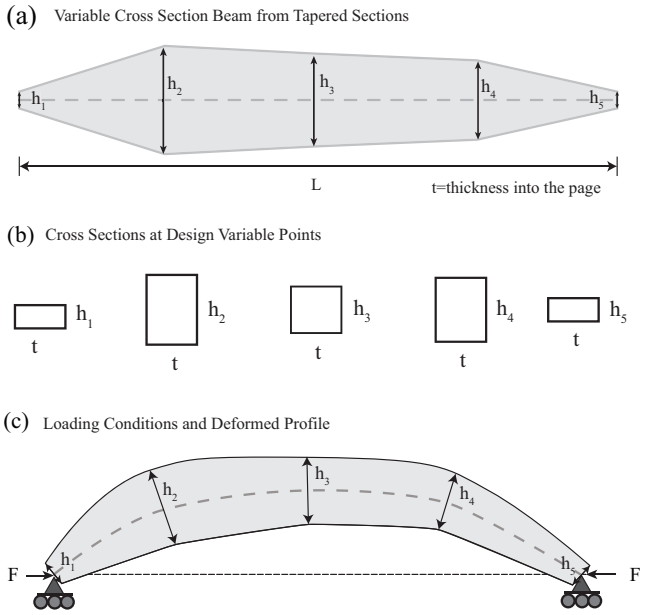


FIGURE 8. A rectangular beam formed from tapered sections with five control points (i.e. $n = 5$) showing (a) h_i, the cross section height at each control point, (b) the cross sections at each control point, and (c) the loading and boundary conditions with the deployed shape.

3.2 Extending the Discrete Model

Multidimensional optimization can be used to extend the discrete model by allowing for the profile error, or error between the desired directrix and the actual deployed directrix, to be minimized for a specified number of torsion springs, n, by efficiently locating the position of the torsion springs. The design variables, d_i where $i = 1$ to n, are the distances of the torsion springs from

one end of the deployed surface as shown in Fig. 9. Constraints can also be introduced such as the maximum angular rotation of a torsional spring and the minimum or maximum lengths of the rigid links. Once a mechanism is decided upon to serve as the torsion spring, further constraints can be imposed to limit stress or size of the mechanism.

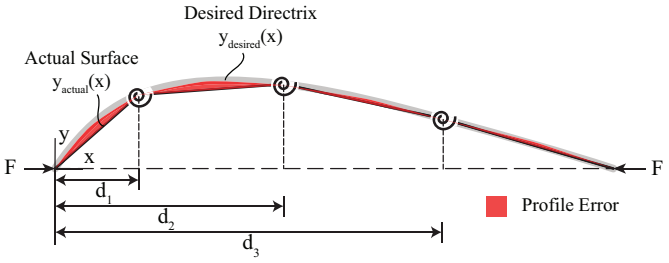


FIGURE 9. The design variables, d_i, are the x coordinate locations of the torsional springs (three shown here), and objective to be minimized, the profile error between the desired and actual surface, for the discrete model.

To illustrate how the discrete model is extended through optimization consider a rigid link system which uses $n/2$ LET joints, that is n pairs of torsion bars, as torsion springs. Thus the number of design variables for the optimization problem is n. The objective function to be minimized is

$$J(d) = Profile\ Error = \int_0^L (y_{desired}(x) - y_{actual}(x))\,dx \quad (15)$$

where $y_{actual}(x)$ is determined directly by the vector of design variables, d.

Several constraints were added to ensure functionality and the ability to be manufactured for the LET joint system. Each link length, L_i was required to be larger than a minimum rigid link length, $MinL$.

$$L_i \geq MinL \quad for\ i = 1 \ldots n+1 \quad (16)$$

The highest stress in any LET joint,θ_i, which is a shear stress occurring in the torsion legs, was constrained to be less than maximum shear stress, $\sigma_{s,max}$.

$$\sigma_i \leq \sigma_{s,max} \quad (17)$$

The length of a torsion leg in any LET joint, $L_{t,i}$, is constrained to be under a maximum value, $MaxL_t$ and above a minimum value, $MinL_t$.

$$MinL_t \leq L_{t,i} \leq MaxL_t \quad for\ i = 1 \ldots n \quad (18)$$

A minimum width of the torsion leg in the LET joint, $Minw$, is enforced.

$$Minw \leq w_i \quad for\ i = 1 \ldots n \quad (19)$$

Constraints are added to ensure the widths of the torsion bars of the LET joints,w_i, fit into the dimensions for the link lengths,L_i, while accounting for the kerf from constructing the LET joints.

$$\begin{gathered} w_1 \leq L_1 - kerf \\ \tfrac{w_i}{2} + \tfrac{w_{i+1}}{2} \leq L_i - kerf \quad for\ i = 2 \ldots n-1 \\ w_n \leq L_n - kerf \end{gathered} \quad (20)$$

The maximum deviation of the system from the desired curve, $MaxDev$, is also added as a constraint.

$$max\,(y_{desired} - y_{actual}) \leq MaxDev \quad (21)$$

The last constraint is implemented as the objective function will aggregate all of the profile error to one area where the curvature of the desired function is the greatest, even if the distance from the desired curve to the actual system becomes large. By imposing a limit on the maximum distance the system can deviate from the desired curve the minimum profile error is slightly increased, but distributed more evenly throughout the system. To gain an appropriate understanding of the range of this constraint the optimization can be performed with a large value for the maximum distance such that the constraint is not binding. The constraint can then be reduced until it reaches at the other extreme a value which will cause the optimization problem to have no feasible solution.

4 Results

The continuous and discrete models were implemented to design deployable parabolic reflectors and the upper surface of a deployable airfoil.

4.1 Continuous Model Implementation

The continuous model extended through optimization was implemented using optimization packages in MATLAB 2014a and ANSYS Mechanical APDL v15.0. The finite element program ANSYS was used to obtain node locations of the final deployed shape to compute the profile error as described by Eq. 12

as well as to obtain a value for the maximum bending stress. A particle swarm algorithm in MATLAB was used to initially find a reasonable solution before switching to an interior-point gradient method to improve the solution. For the gradient method finite differencing was used to obtain the gradients for the objective and constraints. Scaling was also implemented with the profile error and constraints to bring all values on the order of one.

4.1.1 Continuous Model Deployable Parabolic Reflector A deployable parabolic reflector was designed with a desired directrix described by Eq. 6 using a rectangular beam with a variable cross sectional height. The parameters used with the optimization are shown in Table 1. The material properties correspond to those of titanium.

Parameter	Value
Number of design variables (n)	10
Tip Load Force (F)	1 lb
Elastic Modulus (E)	16.5E6 psi
Poisson's Ratio (ν)	0.29
thickness of panel (t)	1 in
Length of beam (L)	10 in
Lowerbound	0.01 in
Upperbound	0.07 in
σ_{yield}	160 ksi

TABLE 1. Optimization parameters for a deployable parabolic surface using the continuous model with a tapered beam finite element model.

The resulting values after the optimization are shown in Table 2. A comparison of the desired shape, the optimized deployed surfaces from the FEA model, and a constant cross section FEA model under the same loading conditions are shown in Fig. 10. As can be seen, the optimization routine optimized the profile to closely match the desired parabolic reflector parabola.

4.1.2 Continuous Model Deployable Airfoil A deployable top surface of the NACA 2215 airfoil with a ten inch chord length was designed using a rectangular beam with a variable cross sectional height. The parameters used with the optimization are the same as those for the deployable parabolic reflector shown in Table 1.



FIGURE 10. Comparison of the desired directrix, the FEA result of the optimized deployed surface, and the FEA result of a constant cross section beam under the same loading conditions. Only half of the desired directrix is shown because of symmetry.

The results after the optimization are shown in Table 3, and a comparison of the optimized deployed surface and the desired airfoil shape are shown in Fig. 11. Considerable error can be seen near the leading edge of the airfoil between the surface and the desired shape. This is due to the profile error only being measured at each control point. This error can be minimized by either computing the profile error at more locations along the surface or increasing the number of control points.

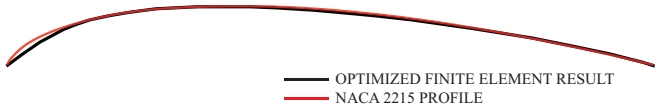


FIGURE 11. Comparison of the FEA result of the optimized deployed surface and the desired NACA 2215 airfoil shape.

4.2 Discrete Model Implementation

4.2.1 Discrete Model Deployable Parabolic Reflector The discrete model was also used to design a deployable parabolic reflector with the same desired directrix as the continuous model. An optimization problem was defined as described in Section 3.2 with the parameters shown in Table 4. The material properties correspond to sheet acrylic.

The resulting values after optimization are described in Table 5. The optimized parabolic reflector was manufactured from acrylic using a laser cutter and is shown in the flat and deployed states is Fig. 12.

4.2.2 Discrete Model Deployable Airfoil A deployable airfoil was designed using the discrete model with optimization in a similar manner to the parabolic reflector. The desired directrix was chosen to be the top surface of a Clark Y airfoil with 10 inch chord length. The optimization parameters were similar to those in Table 4. After the optimization was completed the resulting LET joint pattern was laser cut in acrylic. The pattern is shown in the flat and deployed state in Fig. 13. While the

Parameter	Value
Number of Torsion Springs (n)	10
Tip Load Force (F)	1 lb
Elastic Modulus (E)	400,000 psi
Poisson's Ratio (v)	0.35
thickness of panel (t)	0.115 in
$MinL_t$	2 in
$MaxL_t$	6 in
$Minw$	1/16 in
$kerf$	1/64 in
σ_{max}	9809 psi
$MaxDev$	0.00618 in

TABLE 4. Optimization Parameters for a deployable parabolic surface using the discrete model with LET joints.

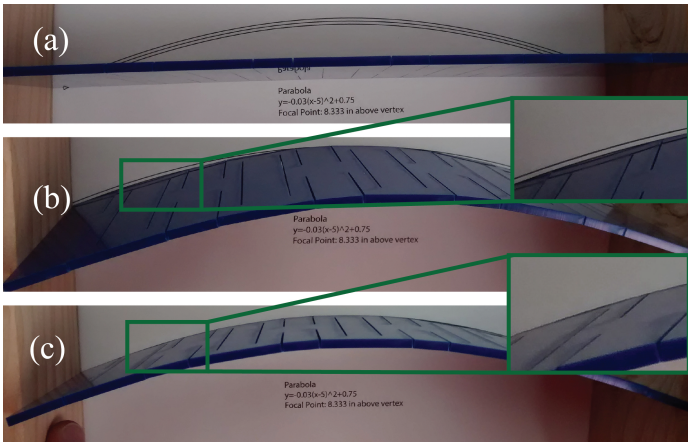


FIGURE 12. Deployable parabolic reflector designed with the discrete model and made of acrylic, where (a) is the desired curve profile with the undeflected prototype, (b) is a comparison control surface made of equally spaced LET joints (note its inability to match the desired parabolic curve when deployed), and (c) is the optimized LET pattern results (note how well the deployed surface matches the desired curve).

structure followed the desired directrix rather closely, some parasitic or unwanted motion occurred due to compression of the LET joints by the tip loads.

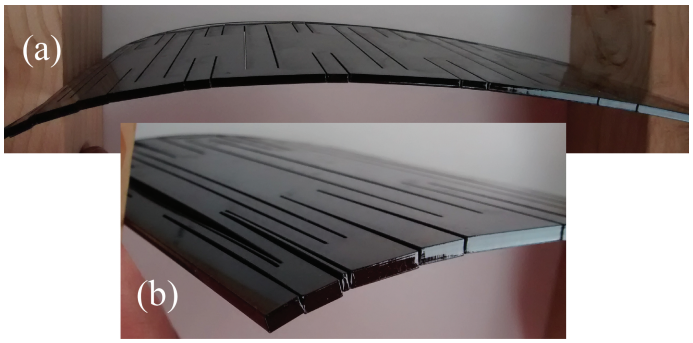


FIGURE 13. Deployable top surface of a Clark Y airfoil designed with the discrete model and made of acrylic, where (a) is the deployed surface and (b) is a detail of the parasitic motion observed in the leading edge.

5 Discussion

Through the creation of the finite-element and physical prototypes several characteristics of both the continuous and discrete models were illuminated. In this section trade-offs between the geometry, material, and tip load actuation forces, how the profile error was measured, and how the models can be implemented into applications will be discussed.

For the continuous model implemented as a rectangular beam with variable cross sectional height, the tip load force can be scaled without affecting the maximum stress level or resulting profile by changing the width of the beam. For both the continuous model using a variable height rectangular beam and the discrete model with a chain of LET joints, if the geometry is preserved but the material is changed the tip force will be scaled corresponding to the change in the modulus.

As was mentioned in the results section for the deployable airfoil made from the continuous model, there was considerable error between the desired directrix and deployed directrix at the leading edge of the airfoil. This error was not reflected in the measure of profile error as the profile error was measured at each control point, and the desired curve and deployed curve matched well at these points. This unaccounted error could be rectified by letting the measure of profile error be determined from more points than just the control points along the curve or by increasing the number of control points. The authors would recommend keeping the number of control points to a minimum and increasing the number of points measured by the profile error calculation to keep the solving time required for the optimization as small as possible. In this manner, a more accurate error could be calculated at very little computational expense, as the final deployed locations at many points are readily available in the finite element model.

The profile error in the discrete model also pushed all of the error between the desired and deployed directrix to the area of greatest curvature of the desired directrix. This was corrected by

placing a constraint on the maximum deviation between the desired directrix and deployed directrix. Other measures of profile error were investigated to achieve a better fit between the two directrices, yet none of these measures performed better than minimizing the area between the curves with a maximum deviation constraint. Further investigation of suitable objective functions to minimize for the discrete model can be carried out in future work.

The continuous model allows for a more exact match between the desired curve and the deflected surface. However, it should be noted that the nodal locations along the center of the rectangular beam rather than the extreme upper surface of the beam were used to compare achieved deflection to desired deflection for the applications in this research. Because of this, the desired directrix will align with the neutral axis of the of the deflected optimized beam rather than along its extreme upper surface. Depending on the application, this may not be a desirable result (if, for example, it is critical for the upper edge of the deflected beam to match the directrix exactly, such as could be the case with a deployed wing with a flexible skin over it). Depending on the needs of the designer, the optimization could be modified so that the upper surface is the surface used for computing the profile error. Such a modification would be fairly simple to implement in a finite element analysis program.

The discrete model constructed with chains of LET joints results in a deployable surface that can function as the final surface as well as a support structure underneath a flexible skin. However, further studies need to be conducted to see how well the deployed surface would behave under various loading conditions, such as a distributed pressure load. Improved resistance to pressure loading could be accomplished by adding a support structure to the deployed surface.

6 Conclusion

Two models, the continuous and discrete models, have been presented as novel ways to create generalized cylindrical deployable surfaces with convex directrices. The continuous model allows for variation in stiffness along the length of the beam or surface such that the resulting curvature when the surface is placed under a tip load matches that of a desired curve. This model lends itself towards morphing ribs which could be covered with a flexible skin to achieve a surface. Multidimensional optimization combined with finite element analysis was used to extend the continuous model to apply constraints and bounds to the model such as a maximum stress constraint. A discrete model was also presented, with demonstration of the model using LET joints as torsion springs. A multidimensional optimization model was used to efficiently locate a particular number of LET joints along the directrix to minimize the error between the desired and actual directrix. Constraints were also enforced to ensure a manufacturable geometry. The feasibility of the continuous model was shown through the creation of FEA models which matched desired curves or directrices under a particular loading condition. The discrete model was shown through the physical creation of a deployable parabolic reflector and deployable airfoil surface. While both models show potential for advancing the design of precise deployable surfaces, further investigation of various loading conditions upon the deployed surfaces and refinement of how the profile error in the optimization procedure is obtained is needed.

ACKNOWLEDGMENT

This material is based on work supported by the National Science Foundation and the Air Force Office of Scientific Research under NSF Grant EFRI-ODISSEI-1240417.

REFERENCES

[1] Zirbel, S. A., Lang, R. J., Thomson, M. W., Sigel, D. A., Walkemeyer, P. E., Trease, B. P., Magleby, S. P., and Howell, L. L., 2013. "Accommodating thickness in origami-based deployable arrays". *Journal of Mechanical Design,* ***135***(11), p. 111005.

[2] Lee, D.-Y., Jung, G.-P., Sin, M.-K., Ahn, S.-H., and Cho, K.-J., 2013. "Deformable wheel robot based on origami structure". In Robotics and Automation (ICRA), 2013 IEEE International Conference on, IEEE, pp. 5612–5617.

[3] Kuribayashi, K., Tsuchiya, K., You, Z., Tomus, D., Umemoto, M., Ito, T., and Sasaki, M., 2006. "Self-deployable origami stent grafts as a biomedical application of ni-rich tini shape memory alloy foil". *Materials Science and Engineering: A,* ***419***(1), pp. 131–137.

[4] Lentink, D., Müller, U., Stamhuis, E., De Kat, R., Van Gestel, W., Veldhuis, L., Henningsson, P., Hedenström, A., Videler, J. J., and Van Leeuwen, J. L., 2007. "How swifts control their glide performance with morphing wings". *Nature,* ***446***(7139), pp. 1082–1085.

[5] Pettit, G. W., Robertshaw, H. H., and Inman, D. J., 2001. "Morphing wings for unmanned aircraft". *Smart Materials Bulletin,* ***2001***(11), pp. 7–12.

[6] Vasista, S., Tong, L., and Wong, K., 2012. "Realization of morphing wings: a multidisciplinary challenge". *Journal of aircraft,* ***49***(1), pp. 11–28.

[7] Wang, H. V., and Rosen, D. W., 2006. "An automated design synthesis method for compliant mechanisms with application to morphing wings". In ASME 2006 IDETC/CIE Conference, American Society of Mechanical Engineers, pp. 231–239.

[8] Yokozeki, T., Takeda, S.-i., Ogasawara, T., and Ishikawa, T., 2006. "Mechanical properties of corrugated composites for candidate materials of flexible wing structures". *Com-*

posites Part A: applied science and manufacturing, ***37***(10), pp. 1578–1586.

[9] Thomson, M. W., 1999. "The astromesh deployable reflector". In Antennas and Propagation Society International Symposium, 1999. IEEE, Vol. 3, IEEE, pp. 1516–1519.

[10] Stern, I., 2003. Deployable reflector antenna with tensegrity support architecture and associated methods, Apr. 1. US Patent 6,542,132.

[11] Tan, L. T., and Pellegrino, S., 2004. "Ultra thin deployable reflector antennas". In Proc. 45th AIAA/ASME/ASCE/AHS/ASC Structures, Structural Dynamics and Materials Conference, pp. 19–22.

[12] Kaplan, R., and Schultz, J. L., 1977. Deployable reflector structure, June 14. US Patent 4,030,102.

[13] Freeland, R., Bilyeu, G., and Veal, G., 1995. "Validation of a unique concept for a low-cost, lightweight space-deployable antenna structure". *Acta Astronautica,* ***35***(9), pp. 565–572.

[14] Jacobsen, J. O., Chen, G., Howell, L. L., and Magleby, S. P., 2009. "Lamina emergent torsional (LET) joint". *Mechanism and Machine Theory,* ***44***(11), pp. 2098–2109.

Results from Continuous Model Optimization for a Parabolic Reflector										
Height of Sections (in)	h_1	h_2	h_3	h_4	h_5	h_6	h_7	h_8	h_9	h_{10}
	0.0261	0.0636	0.0331	0.0645	0.0417	0.0502	0.0539	0.0414	0.0461	0.0397
Other Variables	σ_{max}	ProfileError								
	22.9 ksi	1.70E-6								

TABLE 2. Results from optimization of the continuous model for a deployable parabolic reflector.

Results from Continuous Model Optimization for NACA 2215 top surface										
Height of Sections (in)	h_1	h_2	h_3	h_4	h_5	h_6	h_7	h_8	h_9	h_{10}
	0.0316	0.0227	0.0427	0.0418	0.0664	0.0545	0.0675	0.0583	0.0433	0.0292
Other Variables	σ_{max}	Profile Error								
	53.7 ksi	1.52E-5								

TABLE 3. Results from optimization of the continuous model with variable cross section heights for a deployable NACA 2215 airfoil top surface

Results from Discrete Model Optimization for a Parabolic Reflector											
Horizontal Distances (in)	d_1	d_2	d_3	d_4	d_5	d_6	d_7	d_8	d_9	d_{10}	
	0.91	1.819	2.729	3.638	4.546	5.454	6.362	7.271	8.181	9.090	
Link Lengths (in)	L_1	L_2	L_3	L_4	L_5	L_6	L_7	L_8	L_9	L_{10}	L_{11}
	0.942	0.931	0.921	0.914	0.910	0.909	0.910	0.915	0.921	0.930	0.942
Width (in)	w_1	w_2	w_3	w_4	w_5	w_6	w_7	w_8	w_9	w_{10}	
	0.187	0.276	0.340	0.380	0.401	0.401	.380	.340	0.276	0.187	
Torsion Leg Length (in)	$L_{t,1}$	$L_{t,2}$	$L_{t,3}$	$L_{t,4}$	$L_{t,5}$	$L_{t,6}$	$L_{t,7}$	$L_{t,8}$	$L_{t,9}$	$L_{t,10}$	
	1	1	1	1	1	1	1	1	1	1	
Other Variables	MaxDev	σ_{max}									
	0.00618 in	3,820 psi									

TABLE 5. Results from optimization of the discrete model with LET joints for a deployable parabolic reflector